

Article

Electrospun Resveratrol-Loaded Polyvinylpyrrolidone/Cyclodextrin Nanofibers and Their Biomedical Applications

Ying-Cheng Lin ^{1,2,†}, Stephen Chu-Sung Hu ^{3,4,5,6,7,8,†}, Pao-Hsien Huang ⁹, Tzu-Ching Lin ¹ and Feng-Lin Yen ^{1,5,6,9,10,*}

- ¹ Department of Fragrance and Cosmetic Science, College of Pharmacy, Kaohsiung Medical University, Kaohsiung 807, Taiwan; a5710736@gmail.com (Y.-C.L.); cheng22701@gmail.com (T.-C.L.)
 - ² Graduate Institute of Toxicology, College of Medicine, National Taiwan University, Taipei 100233, Taiwan
 - ³ Department of Dermatology, College of Medicine, Kaohsiung Medical University, Kaohsiung 807, Taiwan; stephen@kmu.edu.tw
 - ⁴ Department of Dermatology, Kaohsiung Medical University Hospital, Kaohsiung 807, Taiwan
 - ⁵ Drug Development and Value Creation Research Center, Kaohsiung Medical University, Kaohsiung 807, Taiwan
 - ⁶ Department of Medical Research, Kaohsiung Medical University Hospital, Kaohsiung 807, Taiwan
 - ⁷ Translational Research Center, Kaohsiung Medical University Hospital, Kaohsiung Medical University, Kaohsiung 807, Taiwan
 - ⁸ Department of Dermatology, Kaohsiung Municipal Siaogang Hospital, Kaohsiung 812, Taiwan
 - ⁹ School of Pharmacy, College of Pharmacy, Kaohsiung Medical University, Kaohsiung 807, Taiwan; j6466497@gmail.com
 - ¹⁰ Institute of Biomedical Sciences, National Sun Yat-Sen University, Kaohsiung 804, Taiwan
- * Correspondence: flyen@kmu.edu.tw; Tel.: +886-7-312-1101 (ext. 2028)
† These authors contributed equally to this work.

Received: 13 May 2020; Accepted: 9 June 2020; Published: 13 June 2020



Abstract: Resveratrol is a naturally occurring polyphenol compound which has been shown to possess antioxidant and anti-inflammatory properties. However, its pharmaceutical applications are limited by its poor water solubility. In this study, we used electrospinning technology to synthesize nanofibers of polyvinylpyrrolidone (PVP) and hydroxypropyl- β -cyclodextrin (HPBCD) loaded with resveratrol. We used X-ray diffractometry to analyze crystalline structure, Fourier transform infrared spectroscopy to determine intermolecular hydrogen bonding, antioxidant assays to measure antioxidant activity, and Franz diffusion cells to evaluate skin penetration. Our results showed that the aqueous solubility of resveratrol nanofibers was greatly improved (by more than 20,000-fold) compared to the pure compound. Analysis of physicochemical properties demonstrated that following nanofiber formation, resveratrol was converted from a crystalline to amorphous structure, and resveratrol formed new intermolecular bonds with PVP and HPBCD. Moreover, resveratrol nanofibers showed good antioxidant activity. In addition, the skin penetration ability of resveratrol in the nanofiber formulation was greater than that of pure resveratrol. Furthermore, resveratrol nanofibers suppressed particulate matter (PM)-induced expression of inflammatory proteins (COX-2 and MMP-9) in HaCaT keratinocytes. Therefore, resveratrol-loaded nanofibers can effectively improve the solubility and physicochemical properties of resveratrol, and may have potential applications as an antioxidant and anti-inflammatory formulation for topical skin application.

Keywords: resveratrol; cyclodextrin; nanofiber; electrospinning; antioxidant activity

1. Introduction

Resveratrol (Res) is a naturally occurring non-flavonoid polyphenol compound and is characterized by a stilbene chemical structure (Figure 1) [1]. It is classified as a phytoalexin, an antimicrobial substance which is synthesized by plants and accumulates around sites of infection [2]. It is known to have antioxidant [3,4], anti-inflammatory [5,6], and antimicrobial properties [7,8]. Resveratrol has also been found to have protective effects on the cardiovascular system [9,10]. Moreover, it has been shown to have anticancer properties in various types of cancers [11–14]. Resveratrol is found in grapes and various other plants, and is also present in red wine. The consumption of red wine by the French people may partially explain the low incidence of coronary heart disease despite high dietary consumption of saturated fats, a phenomenon known as the French paradox [15–17].

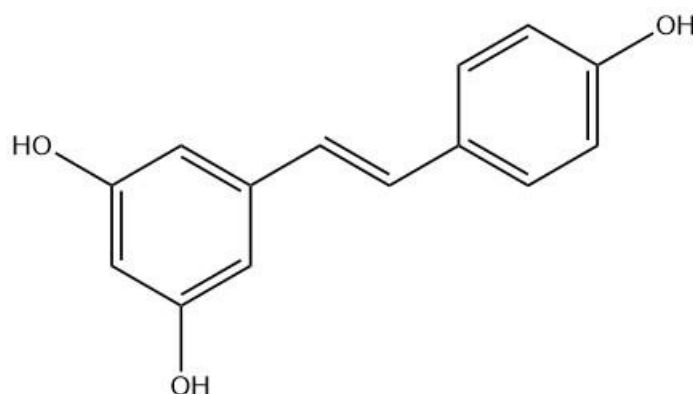


Figure 1. Chemical structure of resveratrol (3,5,4'-trihydroxystilbene).

A major drawback of resveratrol is that it is poorly soluble in water, and can only dissolve in organic solvents such as methanol and ethanol [18,19]. This may decrease its bioavailability and limit its potential applications in the biomedical field. Nanoparticle formulations have been used to improve the solubility of drugs, including liposomes, polymers, gold, silicon and nanofibers [20,21]. In recent years, various studies have attempted to synthesize nanoparticle formulations of resveratrol, in order to improve its water solubility, bioavailability and biological activities [22–26]. For example, nanoformulations of resveratrol have been used in the oncology setting to prevent and treat various types of cancer [27].

Cyclodextrins are generated from the enzymatic degradation of starch. They have a truncated cone structure with a lipophilic inner cavity and hydrophilic outer surface, leading to high aqueous solubility. They can therefore act as nanoparticle sized carriers to improve the water solubility of lipophilic drugs, and enable controlled drug release [28–30]. Naturally occurring cyclodextrins are categorized into α -cyclodextrin (6 glucopyranose units), β -cyclodextrin (7 glucopyranose units), and γ -cyclodextrin (8 glucopyranose units). β -cyclodextrins, such as hydroxypropyl- β -cyclodextrin (HPBCD), are most commonly used as drug nanocarriers due to their optimal cavity size and good drug loading capacity [31,32]. When a drug is included within the cavity of a cyclodextrin, an inclusion complex is generated, thus improving the solubility and stability of the drug [33].

Electrospinning technology uses electrostatic forces to generate nanofibers with very fine diameters [34,35]. There are three main components in the electrospinning system: a high-voltage generator, a syringe with micropump, and a collecting metal plate (such as aluminum foil) [36]. During the electrospinning procedure, the active compound is dissolved in a suitable solvent, and a high molecular weight polymer is added. The solution is transferred into a syringe attached to a micropump, and a high voltage is applied to induce electric charges in the solution [37]. When the electrical forces overcome the surface tension of the solution, a thin liquid jet will leave the syringe tip and travel to the collecting board (containing the opposite charge), and nanoscale fibers are generated as the solvent evaporates [38]. The nanofibers formed by electrospinning technology are characterized by high surface

area to volume ratio, and applications include tissue engineering, biological sensors, wound dressings, and drug carriers [39]. In recent years, electrospinning technology has been increasingly used in the biomedical field, and is becoming a popular area of nanotechnology research [36]. In particular, state-of-the-art developments in electrospinning technology (such as multifluid electrospinning to generate complex nanostructures and Janus structure-based advanced nanofibers) have been used in biomedical applications [40,41].

In this study, we used electrospinning technology to synthesize resveratrol-loaded nanofibers containing different ratios of polyvinylpyrrolidone (PVP) and hydroxypropyl- β -cyclodextrin (HPBCD). We determined whether resveratrol nanofibers can effectively improve the aqueous solubility of resveratrol, analyzed their surface morphology and physicochemical properties, determined their skin penetration ability, and investigated their antioxidant and anti-inflammatory activities.

2. Materials and Methods

2.1. Materials

Resveratrol was obtained from Acetar Bio-Tech Inc. (Xi'an, China). The purity of resveratrol was greater than 97% as determined by high-performance liquid chromatography (HPLC). PVP (average molecular weight 1,300,000 g/mol) was acquired from Sigma-Aldrich (St. Louis, MO, USA). HPBCD was purchased from Zibo Qianhui Biological Technology Co., Ltd (Shandong, China). PM (1649b) was purchased from the National Institute of Standards and Technology (Gaithersburg, MD, USA).

2.2. Electrospinning Procedure

The electrospinning procedure was performed using FES-COS Electro-spinning equipment (Falco Tech Enterprise Co., Taipei, Taiwan). The amount of resveratrol, PVP and HPBCD used to prepare different ratio formulations of resveratrol nanofibers during the electrospinning procedure is presented in Table 1. Firstly, 0.05 g of resveratrol was dissolved in 10 mL of ethanol, and mixed evenly using a magnetic stirrer. HPBCD was then added, and mixed with a magnetic stirrer until it fully dissolved, to ensure that resveratrol had been completely encapsulated by HPBCD. Subsequently, PVP was added, and mixed with a magnetic stirrer till it fully dissolved. The evenly mixed solution was transferred into a syringe with micropump attached. After the electrospinning process, the nanofibers were collected by an aluminum foil. The newly synthesized nanofibers were placed in a sealed plastic bag and stored in a moisture-proof container.

Table 1. Amounts of resveratrol, PVP and HPBCD in different ratio formulations of resveratrol nanofibers.

Ratio (Res:PVP:HPBCD, W/W/W)	Resveratrol (g)	PVP (g)	HPBCD (g)
1:4:20	0.05	0.2	1
1:8:20	0.05	0.4	1
1:16:20	0.05	0.8	1
1:4:40	0.05	0.2	2
1:8:40	0.05	0.4	2
1:16:40	0.05	0.8	2

2.3. High-Performance Liquid Chromatography

High-performance liquid chromatography (HPLC) was performed using a pump with an ultraviolet detector system (Hitachi, Tokyo, Japan). The Mightysil RP-18 GP column (internal diameter of 250 mm \times 4.6 mm, particle size 5 μ m) was used for HPLC (Kanto Corporation, Portland, OR, USA). The mobile phase was composed of acetonitrile : KH_2PO_4 (ratio 35:65, pH 2.8). The flow rate

was 1 mL/min. The eluted resveratrol was detected by an ultraviolet detector (wavelength 290 nm). The absorption peak for resveratrol appeared at 6.57 min.

To obtain the standard calibration curve for HPLC, 1 mg of resveratrol was dissolved in 1 mL methanol, and filtered through a 0.45- μ m membrane. The resveratrol solution was serially diluted to 100, 50, 10, 5, 1, 0.5, 0.1, 0.05, and 0.01 μ g/mL, and analyzed by HPLC. A standard curve for resveratrol was then constructed.

2.4. Determination of Entrapment Efficiency

Firstly, 10 mg of different ratio formulations of resveratrol nanofibers was dissolved in 1 mL methanol, filtered through a 0.45- μ m membrane (Pall Corporation, Port Washington, NY, USA), and diluted 25-fold. The diluted solutions were analyzed by HPLC, and the standard curve was used to calculate the resveratrol amount. The following equation was used to calculate entrapment efficiency [42]:

Resveratrol entrapment efficiency (%) = (Amount of drug in nanofiber / Amount of initially used drug) \times 100%.

2.5. Determination of Aqueous Solubility

Measurement of water solubility was performed at 25 °C temperature and 50 \pm 5% humidity. Pure resveratrol (1 mg) and different ratio formulations of resveratrol nanofibers (containing equivalent of 1 mg resveratrol) were dissolved in 1 mL deionized water, shaken for 1 h (Vortex-Gen 2, Scientific Industries, Bohemia, NY, USA), filtered through a 0.45- μ m membrane (Pall Corporation), and diluted 10-fold. The diluted solutions were analyzed by HPLC, and the standard curve was employed to determine the resveratrol amount.

2.6. Scanning Electron Microscopy

The surface morphology of the nanofiber formulations was visualized using scanning electron microscopy. The nanofibers were sputter coated with gold–palladium and then visualized by a scanning electron microscope (Hitachi S4700, Hitachi, Tokyo, Japan).

2.7. X-Ray Diffractometry

X-ray diffractometry (Siemens D5000, Siemens, Munich, Germany) was used to determine the crystalline versus amorphous structure of pure resveratrol and resveratrol nanofiber formulations. The analysis was conducted using nickel-filtered Cu-K α radiation, using a voltage of 40 kV and current of 25 mA. The range of the angles scanned was from 5° to 50°.

2.8. Fourier Transform Infrared (FTIR) Spectroscopy

The samples (pure resveratrol, PVP, HPBCD and different ratio formulations of resveratrol nanofibers) were mixed with potassium bromide using a mortar, and compressed to form thin sheets. The samples were then analyzed by a FTIR spectrophotometer (Perkin-Elmer Inc., Waltham, MA, USA).

2.9. DPPH Free Radical Scavenging Activity

2,2-diphenyl-1-picrylhydrazyl (DPPH) is a lipophilic free radical, and is soluble in ethanol. It has a purple color, and absorbs light strongly at a wavelength of 517 nm. When DPPH undergoes a redox reaction with an antioxidant, the color of DPPH turns to yellow, and the absorption at 517 nm is decreased [43].

The experimental groups were pure resveratrol in water, pure resveratrol in methanol, resveratrol nanofibers, and vitamin C (as a reference antioxidant). The samples were filtered and serially diluted. To perform the DPPH free radical scavenging assay, 100 μ L of different concentrations of the test

samples was mixed with 100 μL DPPH (200 μM) in a 96-well plate, and incubated in the dark for 30 min. The absorption was then measured using a spectrometer at a wavelength of 517 nm.

2.10. Reducing Power Assay

The production of Prussian blue ($\text{Fe}_4[\text{Fe}(\text{CN})_6]_3$) is used to assess reducing power. For this assay, the Fe^{3+} in $[\text{K}_3\text{Fe}(\text{CN})_6]$ is first reduced by the test sample to Fe^{2+} in $[\text{K}_4\text{Fe}(\text{CN})_6]$, and then the solution is reacted with Fe^{3+} in FeCl_3 to form Prussian blue. The absorption at 700 nm is measured to determine the concentration of Prussian Blue [44].

The reducing power of pure resveratrol and resveratrol nanofibers was evaluated against vitamin C as a reference antioxidant. To perform this assay, 250 μL of the test sample, 250 μL of phosphate buffer (0.2 M), and 250 μL of $\text{K}_3\text{Fe}(\text{CN})_6$ (1%) were mixed in a 1.5-mL microtube at 50 $^\circ\text{C}$ for 20 min, and placed in a cool water bath for 2 min. Then, 250 μL of trichloroacetic acid solution (10%) was added and the solution was centrifuged at 3000 rpm at 4 $^\circ\text{C}$ for 10 min. After centrifugation, 100 μL of supernatant was mixed with 140 μL deionized water and 10 μL $\text{FeCl}_3 \cdot 6\text{H}_2\text{O}$ (0.1%) in a 96-well plate and incubated in the dark for 10 min. The absorption was then measured using a spectrometer at a wavelength of 700 nm.

2.11. ABTS Cation Free Radical Scavenging Activity

When ABTS (2,2'-azino-bis (3-ethylbenzothiazoline-6-sulfonic acid)) is oxidized, it forms a blue-green colored cation free radical ABTS^+ . When an antioxidant test sample is added, ABTS^+ is reduced back to ABTS, and the solution becomes colorless [45].

The ABTS radical scavenging activity of pure resveratrol and resveratrol nanofibers was evaluated against vitamin C as a reference antioxidant. To perform this assay, ABTS (7 mM) was mixed with $\text{K}_2\text{S}_2\text{O}_8$ (2.45 mM) in a 1:1 ratio, and incubated for 12–16 h. The ABTS solution (170 μL) was then mixed with the test sample (30 μL) in a 96-well plate. The absorption was measured using a spectrometer at a wavelength of 734 nm.

2.12. Ex Vivo Skin Penetration

This experiment was performed according to the European Cosmetic Toiletry and Perfumery Association (COLIPA) guideline [46]. The Franz diffusion cell consists of two compartments, the upper donor chamber and the lower receptor chamber. Pig skin from the flank region was cut into 2 cm \times 2 cm pieces and placed between the two chambers, with the stratum corneum facing upwards. The Franz diffusion cell was maintained at 32 $^\circ\text{C}$ and stirred at 600 rpm throughout the experiment. To measure skin penetration, 200 μL of each sample ($n = 6$) was added to the donor chamber. After different amounts of time (1, 2, 4, and 8 h), the pig skin was removed from the Franz diffusion cell. The stratum corneum was obtained by tape stripping. To obtain the epidermal and dermal layers, the skin sample was heated to 85 $^\circ\text{C}$ with a heat pad, and the epidermis and dermis were separated with a scalpel. The samples were immersed in methanol and sonicated for 1 h to extract resveratrol. The content of resveratrol in each sample was determined by the HPLC method.

2.13. Western Blotting

HaCaT cells were cultured in 6-well plates, and treated with pure resveratrol or resveratrol nanofibers. Cells were then harvested, treated with lysis buffer, and proteins were extracted. The proteins were separated by sodium dodecylsulfate–polyacrylamide gel electrophoresis (SDS-PAGE), and then blotted onto polyvinylidene difluoride (PVDF) membranes. The membranes were incubated with antibodies against cyclooxygenase-2 (COX-2) (Santa Cruz Biotechnology, Dallas, TX, USA) and matrix metalloproteinase-9 (MMP-9) (Cell Signaling Technology, Danvers, MA, USA) overnight at 4 $^\circ\text{C}$. Secondary antibodies were then added for 1 h at room temperature, and the immunoreactive bands were visualized with the enhanced chemiluminescence (ECL) system. Antibodies against GAPDH and α -tubulin were used as internal controls.

2.14. Statistical Analysis

Data are shown as mean \pm standard error of the mean (SEM). Comparisons between multiple groups were performed using analysis of variance (ANOVA) with post-hoc Tukey's test. P value < 0.05 was considered to be statistically significant.

3. Results

3.1. Entrapment Efficiency and Aqueous Solubility

Different ratio formulations of resveratrol nanofibers were subjected to HPLC analysis, and the amount of resveratrol was determined from the standard curve. It was found that ratios of 1:4:20, 1:4:40, 1:8:40 and 1:16:40 (Res:PVP:HPBCD) all had greater than 90% entrapment efficiency (Table 2). In particular, the ratio of 1:4:20 produced the greatest entrapment efficiency. In addition, the different ratio formulations of resveratrol nanofibers all had aqueous solubility greater than 800 $\mu\text{g/mL}$, indicating that the nanofiber formulations increased the solubility of resveratrol by more than 20,000-fold.

Table 2. Entrapment efficiency and water solubility of different ratio formulations of resveratrol nanofibers determined by HPLC analysis.

Ratio (Res:PVP:HPBCD, W/W/W)	Entrapment Efficiency (%)	Solubility ($\mu\text{g/mL}$)
1:04:20	98.27 \pm 4.59	894.90 \pm 22.02
1:08:20	84.54 \pm 5.98	875.68 \pm 23.83
1:16:20	79.00 \pm 8.21	855.50 \pm 35.20
1:04:40	97.31 \pm 5.24	860.34 \pm 22.30
1:08:40	96.01 \pm 5.60	900.63 \pm 31.47
1:16:40	90.16 \pm 7.67	896.43 \pm 25.46
Pure resveratrol	-	0.041 \pm 0.001

Results are shown as mean \pm SEM of three independent experiments.

3.2. Surface Morphology of Resveratrol and Resveratrol Nanofibers

Scanning electron microscopy of resveratrol nanofibers showed that a Res:PVP:HPBCD ratio of 1:4:20 produced the thinnest nanofibers (437.96 \pm 41.92 nm) (Table 3, Figure 2). As the proportions of PVP and HPBCD were increased, the diameter of the nanofibers also increased. In particular, when the ratio reached 1:16:40, the structure became fragmented and continuous nanofibers could not be formed. On the other hand, scanning electron microscopy of pure resveratrol showed a clustered particle-like appearance, pure HPBCD exhibited globular structures with cavities, while pure PVP showed plate-like structures.

Table 3. Nanofiber diameter for different ratio formulations of resveratrol nanofibers determined by scanning electron microscopy.

Ratio (Res:PVP:HPBCD, W/W/W)	Nanofiber Diameter (nm)
1:04:20	437.96 \pm 41.92
1:08:20	578.66 \pm 40.11
1:16:20	906.51 \pm 61.85
1:04:40	835.78 \pm 79.57
1:08:40	1259.59 \pm 44.29
1:16:40	2639.59 \pm 157.00

Results are shown as mean \pm SEM.

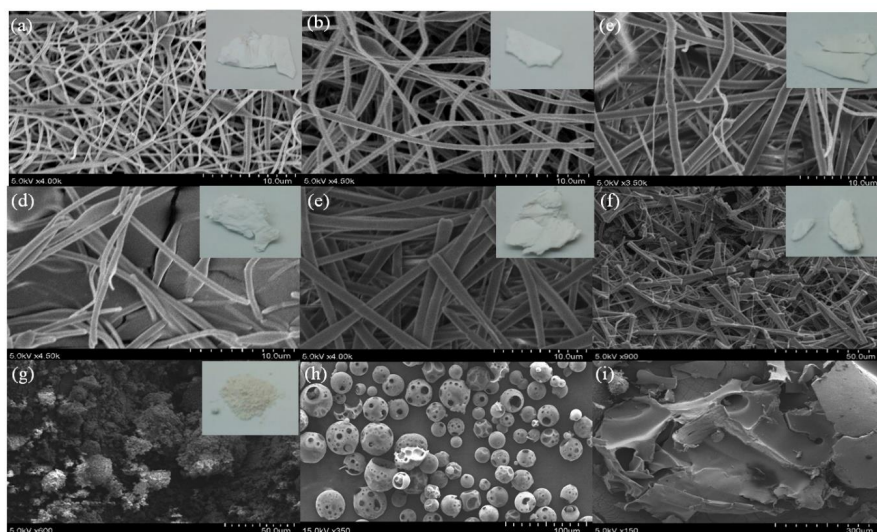


Figure 2. Surface morphology of resveratrol, HPBCD, PVP, and different ratio formulations (Res:PVP:HPBCD) of resveratrol nanofibers, as determined by scanning electron microscopy. (a) 1:4:20, (b) 1:8:20, (c) 1:16:20, (d) 1:4:40, (e) 1:8:40, (f) 1:16:40, (g) pure resveratrol, (h) pure HPBCD, (i) pure PVP.

3.3. Crystalline Versus Amorphous Structure of Resveratrol and Resveratrol Nanofibers

The X-ray diffractometry results showed that pure resveratrol exhibited multiple diffraction peaks at 5° – 30° , indicating that resveratrol had a crystalline structure (Figure 3). On the other hand, the X-ray diffractometry patterns of pure PVP and HPBCD did not display definite diffraction peaks. Following nanofiber formation from the electrospinning procedure (resveratrol nanofibers), the diffraction peaks for resveratrol disappeared and the curves resembled that of PVP and HPBCD. These results showed that following nanofiber formation, resveratrol had been converted from a crystalline to an amorphous structure, indicating that resveratrol had been encapsulated by the nanocarriers.

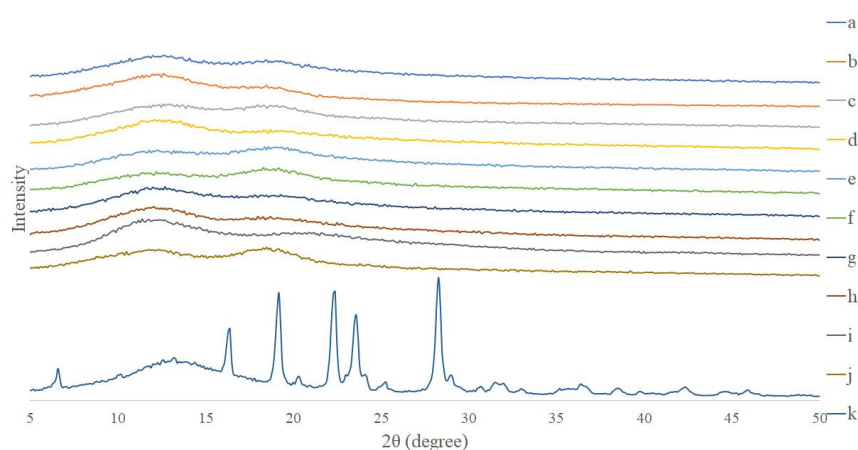


Figure 3. X-ray diffractometry patterns of resveratrol, PVP, HPBCD, and different ratio formulations (Res : PVP : HPBCD) of resveratrol nanofibers. (a) 1:16:40, (b) 1:8:40, (c) 1:4:40, (d) 1:16:20, (e) 1:8:20, (f) 1:4:20, (g) PVP:HPBCD = 1:5 (blank nanofiber), (h) physical mixture of PVP and HPBCD, (i) pure PVP, (j) pure HPBCD, (k) pure resveratrol.

3.4. Intermolecular Chemical Bond Formation Between Resveratrol, HPBCD and PVP

The intermolecular interactions between resveratrol, HPBCD and PVP were analyzed using FTIR. The FTIR spectra showed that pure resveratrol had an absorption band at 3200 – 3500 cm^{-1}

(corresponding to OH functional groups) (Figure 4). PVP showed an absorption band at $1600\sim 1700\text{ cm}^{-1}$ (corresponding to C=O functional group). When resveratrol was complexed with PVP and HPBCD to form resveratrol nanofibers, the absorption band at $3200\sim 3500\text{ cm}^{-1}$ was broadened (indicating formation of new hydrogen bonds with nanocarriers), and there was an absorption band at $1600\sim 1700\text{ cm}^{-1}$ (corresponding to C=O functional group of PVP). These results indicate that resveratrol had formed new intermolecular bonds, and had been encapsulated by its nanocarriers.

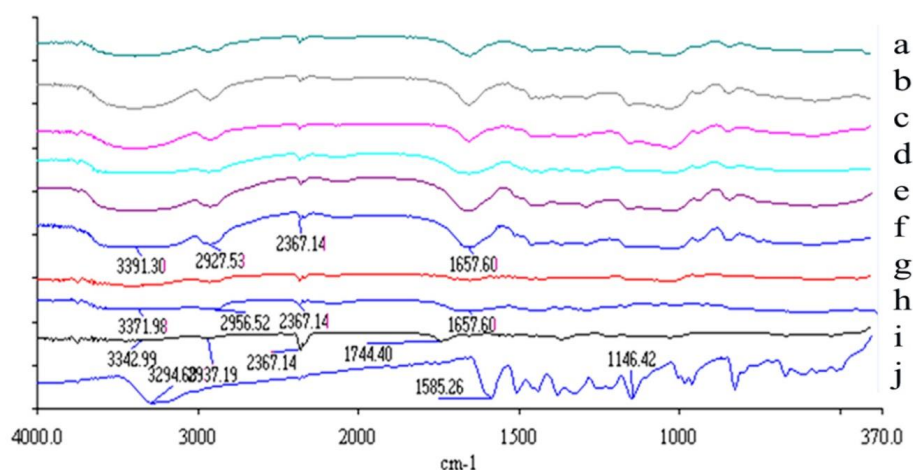


Figure 4. Fourier transform infrared (FTIR) spectra for resveratrol, PVP, HPBCD, and different ratio formulations (Res:PVP:HPBCD) of resveratrol nanofibers. (a) 1:16:40, (b) 1:8:40, (c) 1:4:40, (d) 1:16:20, (e) 1:8:20, (f) 1:4:20, (g) physical mixture of PVP and HPBCD, (h) pure PVP, (i) pure HPBCD, (j) pure resveratrol.

3.5. DPPH Free Radical Scavenging Activity

The *in vitro* antioxidant assays were performed using a ratio of 1:4:20 for resveratrol nanofibers. The results from the DPPH assay showed that the free radical scavenging activity of resveratrol nanofibers was greater than that of pure resveratrol in methanol, and equivalent to that of vitamin C (Figure 5). This indicates that the antioxidant activity of resveratrol was improved following nanofiber formation. The pure resveratrol in water formulation showed low DPPH free radical scavenging activity, likely due to the poor water solubility of resveratrol.

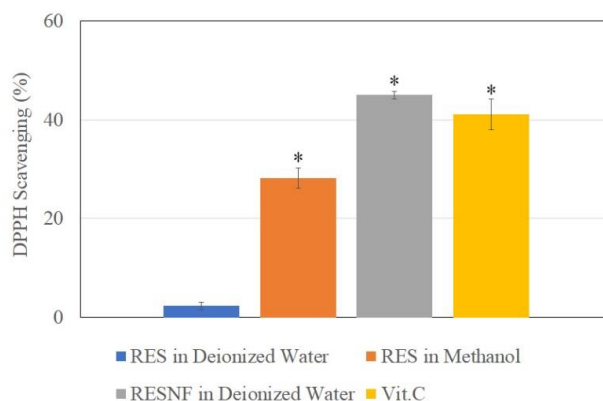


Figure 5. DPPH free radical scavenging activity of resveratrol in deionized water, resveratrol in methanol, resveratrol nanofibers (RESNF) in deionized water, and vitamin C at $10\text{ }\mu\text{g/mL}$ concentration. Results are shown as mean \pm SEM of three independent experiments. * represents $P < 0.05$ when compared to resveratrol in deionized water.

3.6. Reducing Power

The results from the reducing power assay (production of Prussian blue) showed that the reducing power of pure resveratrol in methanol and resveratrol nanofibers was similar and equivalent to that of vitamin C (Figure 6). Therefore, resveratrol retained its reducing power following nanofiber formation. On the other hand, pure resveratrol in water showed low reducing power, likely due to the poor aqueous solubility of resveratrol.

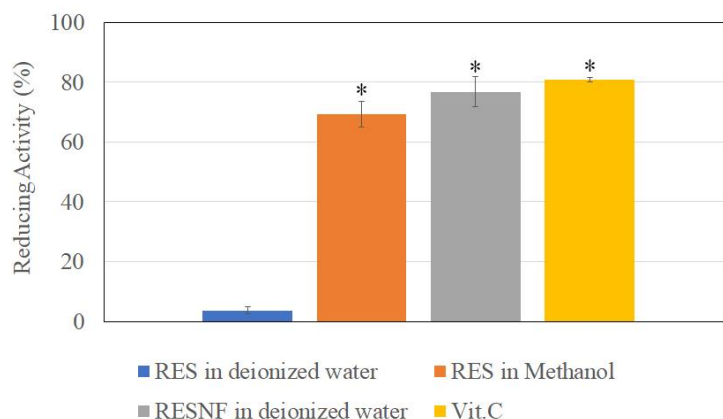


Figure 6. Reducing power of resveratrol in deionized water, resveratrol in methanol, resveratrol nanofibers (RESNF) in deionized water, and vitamin C at 20 $\mu\text{g}/\text{mL}$ concentration. Results are shown as mean \pm SEM of three independent experiments. * represents $P < 0.05$ when compared to resveratrol in deionized water.

3.7. ABTS Cation Free Radical Scavenging Activity

The ABTS free radical scavenging activity of pure resveratrol in methanol and resveratrol nanofibers was similar and equivalent to that of vitamin C (Figure 7). This indicates that resveratrol retained its ABTS free radical scavenging activity following nanofiber formation. On the other hand, pure resveratrol in water showed low ABTS scavenging activity, likely due to the poor solubility of resveratrol in water.

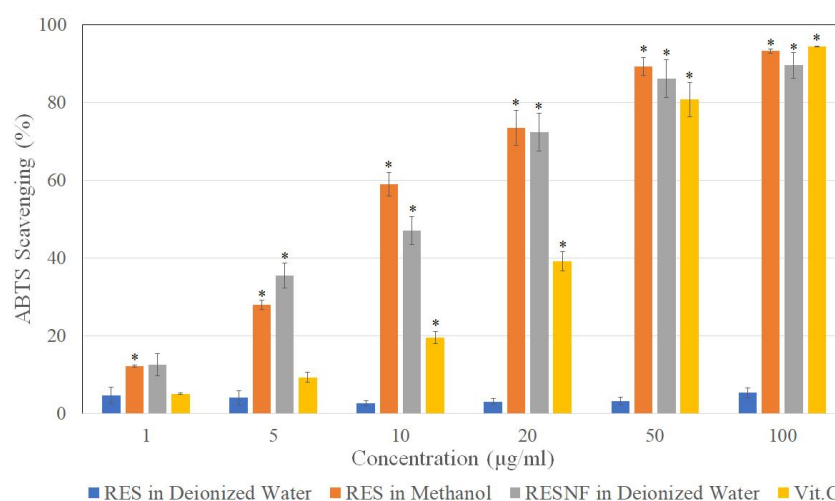


Figure 7. ABTS free radical scavenging activity of resveratrol in deionized water, resveratrol in methanol, resveratrol nanofibers (RESNF) in deionized water, and vitamin C at various concentrations. Results are shown as mean \pm SEM of three independent experiments. * represents $P < 0.05$ when compared to resveratrol in deionized water.

3.8. Ex Vivo Skin Penetration

We next investigated whether the skin penetration ability of resveratrol is increased after nanofiber formation. Pig skin was exposed to pure resveratrol or resveratrol nanofibers, and different layers of the skin (stratum corneum, epidermis, dermis) were collected at 1, 2 and 4 and 8 h to determine drug concentration. The results demonstrated that resveratrol in the nanofiber formulation showed greater penetration into the epidermis and dermis compared with pure resveratrol, and this occurred in a time-dependent manner (Figure 8). Therefore, nanofiber formulations of resveratrol may increase the skin penetration of resveratrol.

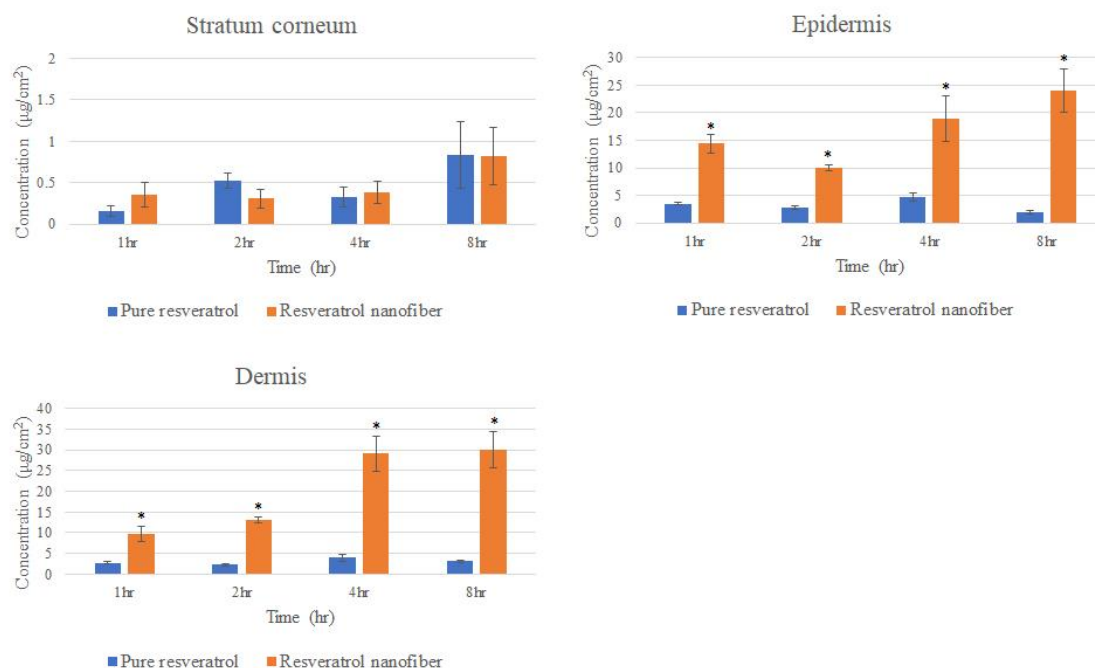


Figure 8. Effects of pure resveratrol and resveratrol nanofibers on skin penetration through pig skin. The amount of drug in the stratum corneum, epidermis and dermis at various time points were determined. Results are shown as mean \pm SEM ($n = 6$). * represents $P < 0.05$ when compared to pure resveratrol.

3.9. Effects of Resveratrol Nanofibers on Particulate Matter (PM)-Induced Inflammatory Proteins Expression in HaCaT Keratinocytes

Western blotting showed that treatment of HaCaT keratinocytes with PM ($50 \mu\text{g}/\text{cm}^2$) led to increased protein expression of inflammatory proteins COX-2 and MMP-9 (Figure 9). Treatment of HaCaT keratinocytes with pure resveratrol in PBS ($20 \mu\text{M}$) had no significant effect on the expression levels of these proteins, which may be due to the poor aqueous solubility of resveratrol. On the other hand, treatment of HaCaT cells with pure resveratrol in DMSO ($20 \mu\text{M}$) and resveratrol nanofibers ($20 \mu\text{M}$) suppressed PM-induced expression of COX-2 and MMP-9. Therefore, resveratrol retained its anti-inflammatory effects following nanofiber formation.

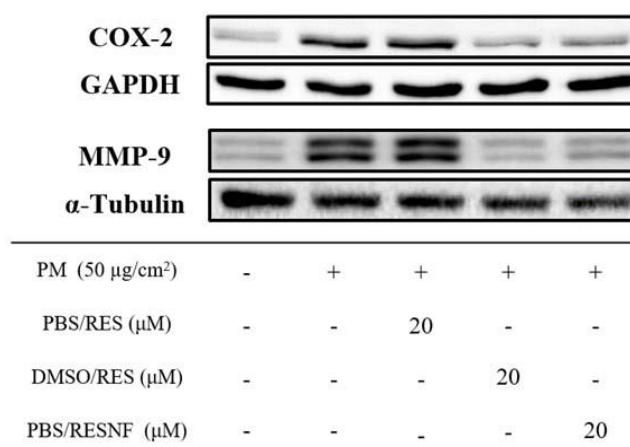


Figure 9. Western blots demonstrating the effects of pure resveratrol in PBS (PBS/RES), pure resveratrol in DMSO (DMSO/RES) and resveratrol nanofibers in PBS (PBS/RESNF) on particulate matter (PM)-induced protein expression of COX-2 (24 h) and MMP-9 (24 h) in HaCaT keratinocytes. Blots are representative of three independent experiments.

4. Discussion

Nanofibers generated from electrospinning technology have been increasingly used as drug delivery systems [37,38,47]. In this study, we synthesized nanofibers of PVP and cyclodextrin (HPBCD) loaded with resveratrol, in order to improve the solubility and physicochemical properties of the drug. The use of nanofibers as drug carriers present several advantages, including high loading capacity and encapsulation efficiency, and a high surface area to volume ratio leading to increased dissolution rate. PVP is chosen as a nanocarrier in this study since it is characterized by high water solubility, rapid dissolution and low toxicity [48–50]. However, PVP is highly hygroscopic and its nanofibers are unstable in atmospheric conditions [50]. Blending HPBCD with PVP can reduce the hygroscopicity of PVP and improve the stability of the nanofibers [51]. Previously, nanofiber formulations combining active compounds with PVP and HPBCD have been synthesized using electrospinning technology [50–53].

In this study, we found that resveratrol can be complexed with HPBCD/PVP and subjected to the electrospinning procedure to form stable nanofibers. The electrospinning process achieved good entrapment efficiency, and the water solubility of resveratrol nanofibers was greatly increased compared to the pure compound. HPBCD is a cyclodextrin with high water solubility, and is characterized by a lipophilic inner cavity and hydrophilic outer surface [54]. The inclusion of resveratrol into the cavity of HPBCD to form a cyclodextrin inclusion complex may explain the greatly increased aqueous solubility of resveratrol [33]. Moreover, the encapsulation of resveratrol by the nanocarrier PVP may lead to improved water solubility. For future work, it will be important to test the *in vitro* release profile of resveratrol from nanofibers, in order to gain further insight into the pharmaceutical properties of this drug formulation.

Scanning electron microscopy showed that resveratrol nanofibers with low proportions of PVP and HPBCD (for example, Res:PVP:HPBCD ratio of 1:4:20) produced the thinnest nanofibers. On the other hand, resveratrol nanofibers with high proportions of PVP and HPBCD (in particular 1:16:40) produced thicker fibers which became fragmented. A possible explanation is that when the proportions of PVP and HPBCD increase, the viscosity of the nanofibers also increases [50,55], which may lead to the formation of thicker fibers. In addition, the formation of intermolecular bonds between resveratrol and HPBCD/PVP may stabilize the nanofiber structure, enabling the formation of thin continuous nanofibers.

The improvement in water solubility of resveratrol may be a result of changes in physicochemical properties. An analysis of the physicochemical properties by X-ray diffractometry demonstrated that

following nanofiber formation, resveratrol was converted from a crystalline to amorphous structure. In addition, FTIR showed that new intermolecular bonds (including hydrogen bonds) were formed between resveratrol and HPBCD/PVP. These results indicate that resveratrol had been encapsulated by the nanocarriers, and the formation of nanofibers improved the physicochemical properties of resveratrol. Previous reports have also demonstrated that when a drug is loaded into PVP/HPBCD nanofibers, it is converted from crystalline to amorphous form, and new intermolecular bonds are formed between the drug and nanocarriers [50,51].

Moreover, we demonstrated that resveratrol nanofibers possess good DPPH free radical scavenging activity, reducing power, and ABTS radical scavenging activity, indicating that resveratrol may show improved antioxidant activity following nanofiber formation [3]. Furthermore, the antioxidant activities of resveratrol nanofibers are equivalent to that of vitamin C, which is known as a strong natural antioxidant [56]. Therefore, nanofiber formulations of resveratrol not only show greatly improved water solubility, but exhibit good antioxidant activity as well. Our results indicate that resveratrol-loaded PVP/HPBCD nanofibers may have potential clinical applications as an antioxidant formulation in the future.

In order to exert biological effects on the skin, cutaneous drug formulations need to penetrate the different layers of skin. The stratum corneum has been shown to be a rate-limiting factor for the skin penetration of drugs [57]. In this study, pig skin was used to investigate skin penetration, since it exhibits cutaneous barrier function similar to human skin [58]. Our results demonstrated that, compared to pure resveratrol, resveratrol in the nanofiber formulation showed greater penetration through the stratum corneum and into the epidermal and dermal layers. Therefore, resveratrol nanofibers may be a suitable cutaneous drug formulation.

Previously, it has been shown that particulate matter (PM) in air pollution may exert inflammatory effects on the skin [59–62]. Therefore, we used PM-induced HaCaT keratinocyte inflammation as an *in vitro* model to investigate the potential anti-inflammatory effects of resveratrol nanofibers. Proteins which have been shown to play important roles in inflammation include COX-2 [63] and MMP-9 [64–66]. Our results showed that resveratrol nanofibers suppressed particulate matter (PM)-induced expression of inflammatory proteins COX-2 and MMP-9 in keratinocytes. Therefore, resveratrol nanofibers may be a potential anti-inflammatory drug formulation for skin.

Based on the results of this study, we propose that resveratrol nanofibers may be a suitable cosmetic or drug formulation for topical skin application. The nanofibers may be applied to the skin as a thin film with local actions on the skin, for example as a facial mask product. The high surface area to volume ratio of the nanofiber facial mask may facilitate drug delivery to facial skin, leading to antioxidant and anti-inflammatory actions. Previously, facial masks formed from electrospun fiber mats have been developed to exert an anti-wrinkle effect on facial skin [67]. Since oxidative stress and chronic inflammation are known to play important roles in skin aging [68], resveratrol nanofibers may be a potential anti-aging cosmetic formulation.

In conclusion, resveratrol-loaded nanofibers can effectively improve the aqueous solubility and physicochemical properties of resveratrol, show enhanced skin penetration, and exhibit antioxidant and anti-inflammatory properties. Therefore, resveratrol nanofibers may have potential applications as an antioxidant and anti-inflammatory formulation for topical skin application in the future.

Author Contributions: Conceptualization, F.-L.Y. and S.C.-S.H.; methodology, F.-L.Y.; formal analysis, F.-L.Y., Y.-C.L., P.-H.H., T.-C.L. and S.C.-S.H.; investigation, F.-L.Y., Y.-C.L., P.-H.H. and T.-C.L.; data curation, F.-L.Y. and Y.-C.L.; writing—original draft preparation, F.-L.Y. and S.C.-S.H.; writing—review and editing, F.-L.Y. and S.C.-S.H.; funding acquisition, F.-L.Y. All authors have read and agreed to the published version of the manuscript.

Funding: This research was funded by grants from the Ministry of Science and Technology, Taiwan (MOST 108-2622-8-037-002-, 108-2314-B-037-086-), Kaohsiung Medical University Drug Development and Value Creation Research Center (KMU-TC108A03-10), Kaohsiung Medical University Hospital (KMUH108-8R58) and Kaohsiung Medical University Research Center Grant (KMU-TC108A01-1).

Conflicts of Interest: The authors declare no conflict of interest.

References

1. Gambini, J.; Ingles, M.; Olaso, G.; Lopez-Grueso, R.; Bonet-Costa, V.; Gimeno-Mallench, L.; Mas-Bargues, C.; Abdelaziz, K.M.; Gomez-Cabrera, M.C.; Vina, J.; et al. Properties of resveratrol: In Vitro and In Vivo studies about metabolism, bioavailability, and biological effects in animal models and humans. *Oxidative Med. Cell. Longev.* **2015**, *2015*, 837042. [[CrossRef](#)] [[PubMed](#)]
2. Cucciolla, V.; Borriello, A.; Oliva, A.; Galletti, P.; Zappia, V.; Della Ragione, F. Resveratrol: From basic science to the clinic. *Cell Cycle* **2007**, *6*, 2495–2510. [[CrossRef](#)] [[PubMed](#)]
3. Carrizzo, A.; Forte, M.; Damato, A.; Trimarco, V.; Salzano, F.; Bartolo, M.; Maciag, A.; Puca, A.A.; Vecchione, C. Antioxidant effects of resveratrol in cardiovascular, cerebral and metabolic diseases. *Food Chem. Toxicol.* **2013**, *61*, 215–226. [[CrossRef](#)] [[PubMed](#)]
4. He, S.; Yan, X. From resveratrol to its derivatives: New sources of natural antioxidant. *Curr. Med. Chem.* **2013**, *20*, 1005–1017. [[PubMed](#)]
5. Csiszar, A. Anti-inflammatory effects of resveratrol: Possible role in prevention of age-related cardiovascular disease. *Ann. N. Y. Acad. Sci.* **2011**, *1215*, 117–122. [[CrossRef](#)]
6. Zhang, F.; Liu, J.; Shi, J.S. Anti-inflammatory activities of resveratrol in the brain: Role of resveratrol in microglial activation. *Eur. J. Pharmacol.* **2010**, *636*, 1–7. [[CrossRef](#)]
7. Hwang, D.; Lim, Y.H. Resveratrol antibacterial activity against *Escherichia coli* is mediated by Z-ring formation inhibition via suppression of FtsZ expression. *Sci. Rep.* **2015**, *5*, 10029. [[CrossRef](#)]
8. Ferreira, S.; Domingues, F. The antimicrobial action of resveratrol against *Listeria monocytogenes* in food-based models and its antibiofilm properties. *J. Sci. Food Agric.* **2016**, *96*, 4531–4535. [[CrossRef](#)]
9. Wu, J.M.; Wang, Z.R.; Hsieh, T.C.; Bruder, J.L.; Zou, J.G.; Huang, Y.Z. Mechanism of cardioprotection by resveratrol, a phenolic antioxidant present in red wine (Review). *Int. J. Mol. Med.* **2001**, *8*, 3–17. [[CrossRef](#)]
10. Zordoky, B.N.; Robertson, I.M.; Dyck, J.R. Preclinical and clinical evidence for the role of resveratrol in the treatment of cardiovascular diseases. *Biochim. Et Biophys. Acta* **2015**, *1852*, 1155–1177. [[CrossRef](#)]
11. Aziz, S.W.; Aziz, M.H. Protective molecular mechanisms of Resveratrol in UVR induced Skin carcinogenesis. *Photodermatol. Photoimmunol. Photomed.* **2017**. [[CrossRef](#)] [[PubMed](#)]
12. Whitlock, N.C.; Baek, S.J. The anticancer effects of resveratrol: Modulation of transcription factors. *Nutr. Cancer* **2012**, *64*, 493–502. [[CrossRef](#)] [[PubMed](#)]
13. Hsieh, T.C.; Wu, J.M. Resveratrol: Biological and pharmaceutical properties as anticancer molecule. *Biofactors* **2010**, *36*, 360–369. [[CrossRef](#)] [[PubMed](#)]
14. Jang, M.; Cai, L.; Udeani, G.O.; Slowing, K.V.; Thomas, C.F.; Beecher, C.W.; Fong, H.H.; Farnsworth, N.R.; Kinghorn, A.D.; Mehta, R.G.; et al. Cancer chemopreventive activity of resveratrol, a natural product derived from grapes. *Science* **1997**, *275*, 218–220. [[CrossRef](#)]
15. Catalgol, B.; Batirel, S.; Taga, Y.; Ozer, N.K. Resveratrol: French paradox revisited. *Front. Pharmacol.* **2012**, *3*, 141. [[CrossRef](#)]
16. Vidavalur, R.; Otani, H.; Singal, P.K.; Maulik, N. Significance of wine and resveratrol in cardiovascular disease: French paradox revisited. *Exp. Clin. Cardiol.* **2006**, *11*, 217–225.
17. Kopp, P. Resveratrol, a phytoestrogen found in red wine. A possible explanation for the conundrum of the 'French paradox'? *Eur. J. Endocrinol.* **1998**, *138*, 619–620. [[CrossRef](#)]
18. Bolko, K.; Zvonar, A.; Gasperlin, M. Mixed lipid phase SMEDDS as an innovative approach to enhance resveratrol solubility. *Drug Dev. Ind. Pharm.* **2014**, *40*, 102–109. [[CrossRef](#)]
19. Balata, G.F.; Essa, E.A.; Shamardl, H.A.; Zaidan, S.H.; Abourehab, M.A. Self-emulsifying drug delivery systems as a tool to improve solubility and bioavailability of resveratrol. *Drug Des. Dev. Ther.* **2016**, *10*, 117–128. [[CrossRef](#)]
20. Watkins, R.; Wu, L.; Zhang, C.; Davis, R.M.; Xu, B. Natural product-based nanomedicine: Recent advances and issues. *Int. J. Nanomed.* **2015**, *10*, 6055–6074. [[CrossRef](#)]
21. Bozzuto, G.; Molinari, A. Liposomes as nanomedical devices. *Int. J. Nanomed.* **2015**, *10*, 975–999. [[CrossRef](#)] [[PubMed](#)]
22. Jeon, Y.O.; Lee, J.S.; Lee, H.G. Improving solubility, stability, and cellular uptake of resveratrol by nanoencapsulation with chitosan and gamma-poly (glutamic acid). *Colloids Surf. B Biointerfaces* **2016**, *147*, 224–233. [[CrossRef](#)] [[PubMed](#)]

23. Feng, M.; Zhong, L.X.; Zhan, Z.Y.; Huang, Z.H.; Xiong, J.P. Enhanced antitumor efficacy of resveratrol-loaded nanocapsules in colon cancer cells: Physicochemical and biological characterization. *Eur. Rev. Med. Pharmacol. Sci.* **2017**, *21*, 375–382. [[PubMed](#)]
24. Carletto, B.; Berton, J.; Ferreira, T.N.; Dalmolin, L.F.; Paludo, K.S.; Mainardes, R.M.; Farago, P.V.; Favero, G.M. Resveratrol-loaded nanocapsules inhibit murine melanoma tumor growth. *Colloids Surf. B Biointerfaces* **2016**, *144*, 65–72. [[CrossRef](#)] [[PubMed](#)]
25. Summerlin, N.; Qu, Z.; Pujara, N.; Sheng, Y.; Jambhrunkar, S.; McGuckin, M.; Popat, A. Colloidal mesoporous silica nanoparticles enhance the biological activity of resveratrol. *Colloids Surf. B Biointerfaces* **2016**, *144*, 1–7. [[CrossRef](#)] [[PubMed](#)]
26. Park, S.Y.; Chae, S.Y.; Park, J.O.; Lee, K.J.; Park, G. Gold-conjugated resveratrol nanoparticles attenuate the invasion and MMP-9 and COX-2 expression in breast cancer cells. *Oncol. Rep.* **2016**, *35*, 3248–3256. [[CrossRef](#)] [[PubMed](#)]
27. Siddiqui, I.A.; Sanna, V.; Ahmad, N.; Sechi, M.; Mukhtar, H. Resveratrol nanoformulation for cancer prevention and therapy. *Ann. N. Y. Acad. Sci.* **2015**, *1348*, 20–31. [[CrossRef](#)]
28. Szente, L.; Szejtli, J. Highly soluble cyclodextrin derivatives: Chemistry, properties, and trends in development. *Adv. Drug Deliv. Rev.* **1999**, *36*, 17–28. [[CrossRef](#)]
29. Tiwari, G.; Tiwari, R.; Rai, A.K. Cyclodextrins in delivery systems: Applications. *J. Pharm. Bioallied Sci.* **2010**, *2*, 72–79. [[CrossRef](#)]
30. Loftsson, T.; Jarho, P.; Masson, M.; Jarvinen, T. Cyclodextrins in drug delivery. *Expert Opin. Drug Deliv.* **2005**, *2*, 335–351. [[CrossRef](#)]
31. Challa, R.; Ahuja, A.; Ali, J.; Khar, R.K. Cyclodextrins in drug delivery: An updated review. *AAPS PharmSciTech* **2005**, *6*, E329–E357. [[CrossRef](#)] [[PubMed](#)]
32. Rajewski, R.A.; Stella, V.J. Pharmaceutical applications of cyclodextrins. 2. In vivo drug delivery. *J. Pharm. Sci.* **1996**, *85*, 1142–1169. [[CrossRef](#)] [[PubMed](#)]
33. Gidwani, B.; Vyas, A. A comprehensive review on cyclodextrin-based carriers for delivery of chemotherapeutic cytotoxic anticancer drugs. *Biomed. Res. Int.* **2015**, *2015*, 198268. [[CrossRef](#)] [[PubMed](#)]
34. Ye, K.; Kuang, H.; You, Z.; Morsi, Y.; Mo, X. Electrospun nanofibers for tissue engineering with drug loading and release. *Pharmaceutics* **2019**, *11*, 182. [[CrossRef](#)]
35. Han, X.; Huo, P.; Ding, Z.; Kumar, P.; Liu, B. Preparation of lutein-loaded PVA/sodium alginate nanofibers and investigation of its release behavior. *Pharmaceutics* **2019**, *11*, 449. [[CrossRef](#)]
36. Bhardwaj, N.; Kundu, S.C. Electrospinning: A fascinating fiber fabrication technique. *Biotechnol. Adv.* **2010**, *28*, 325–347. [[CrossRef](#)]
37. Hu, X.; Liu, S.; Zhou, G.; Huang, Y.; Xie, Z.; Jing, X. Electrospinning of polymeric nanofibers for drug delivery applications. *J. Control. Release Off. J. Control. Release Soc.* **2014**, *185*, 12–21. [[CrossRef](#)]
38. Chew, S.Y.; Wen, Y.; Dzenis, Y.; Leong, K.W. The role of electrospinning in the emerging field of nanomedicine. *Curr. Pharm. Des.* **2006**, *12*, 4751–4770. [[CrossRef](#)]
39. Teo, W.E.; Inai, R.; Ramakrishna, S. Technological advances in electrospinning of nanofibers. *Sci. Technol. Adv. Mater.* **2011**, *12*, 013002. [[CrossRef](#)]
40. Yu, D.G.; Wang, M.; Li, X.; Liu, X.; Zhu, L.M.; Annie Bligh, S.W. Multifluid electrospinning for the generation of complex nanostructures. *Wiley Interdiscip. Rev. Nanomed. Nanobiotechnol.* **2020**, *12*, e1601. [[CrossRef](#)]
41. Yang, J.; Wang, K.; Yu, D.G.; Yang, Y.; Bligh, S.W.A.; Williams, G.R. Electrospun Janus nanofibers loaded with a drug and inorganic nanoparticles as an effective antibacterial wound dressing. *Mater. Sci. Eng. C Mater. Biol. Appl.* **2020**, *111*, 110805. [[CrossRef](#)] [[PubMed](#)]
42. Lazaridou, M.; Christodoulou, E.; Nerantzaki, M.; Kostoglou, M.; Lambropoulou, D.A.; Katsarou, A.; Pantopoulos, K.; Bikiaris, D.N. Formulation and In-Vitro characterization of chitosan-nanoparticles loaded with the iron chelator deferoxamine mesylate (DFO). *Pharmaceutics* **2020**, *12*, 238. [[CrossRef](#)] [[PubMed](#)]
43. Kedare, S.B.; Singh, R.P. Genesis and development of DPPH method of antioxidant assay. *J. Food Sci. Technol.* **2011**, *48*, 412–422. [[CrossRef](#)]
44. Ak, T.; Gülçin, I. Antioxidant and radical scavenging properties of curcumin. *Chem. Biol. Interact.* **2008**, *174*, 27–37. [[CrossRef](#)]
45. Re, R.; Pellegrini, N.; Proteggente, A.; Pannala, A.; Yang, M.; Rice-Evans, C. Antioxidant activity applying an improved ABTS radical cation decolorization assay. *Free Radic. Biol. Med.* **1999**, *26*, 1231–1237. [[CrossRef](#)]

46. Cosmetics_Europe. COLIPA Guidelines: Guidelines for Percutaneous Absorption/Penetration. 1997. Available online: https://www.cosmeticseurope.eu/files/8314/6407/9075/Guidelines_for_Percutaneous_Absorption-Penetration_-_1997.pdf (accessed on 2 June 2020).
47. Martínez-Ortega, L.; Mira, A.; Fernandez-Carvajal, A.; Mateo, C.R.; Mallavia, R.; Falco, A. Development of a new delivery system based on drug-loadable electrospun nanofibers for psoriasis treatment. *Pharmaceutics* **2019**, *11*, 14. [[CrossRef](#)]
48. Karavas, E.; Georgarakis, M.; Docoslis, A.; Bikiaris, D. Combining SEM, TEM, and micro-Raman techniques to differentiate between the amorphous molecular level dispersions and nanodispersions of a poorly water-soluble drug within a polymer matrix. *Int. J. Pharm.* **2007**, *340*, 76–83. [[CrossRef](#)]
49. Wu, K.; Li, J.; Wang, W.; Winstead, D.A. Formation and characterization of solid dispersions of piroxicam and polyvinylpyrrolidone using spray drying and precipitation with compressed antisolvent. *J. Pharm. Sci.* **2009**, *98*, 2422–2431. [[CrossRef](#)]
50. Samprasit, W.; Akkaramongkolporn, P.; Ngawhirunpat, T.; Rojanarata, T.; Kaomongkolgit, R.; Opanasopit, P. Fast releasing oral electrospun PVP/CD nanofiber mats of taste-masked meloxicam. *Int. J. Pharm.* **2015**, *487*, 213–222. [[CrossRef](#)]
51. Tonglairoum, P.; Ngawhirunpat, T.; Rojanarata, T.; Kaomongkolgit, R.; Opanasopit, P. Fast-acting clotrimazole composited PVP/HPbetaCD nanofibers for oral candidiasis application. *Pharm. Res.* **2014**, *31*, 1893–1906. [[CrossRef](#)]
52. Tonglairoum, P.; Ngawhirunpat, T.; Rojanarata, T.; Panomsuk, S.; Kaomongkolgit, R.; Opanasopit, P. Fabrication of mucoadhesive chitosan coated polyvinylpyrrolidone/cyclodextrin/clotrimazole sandwich patches for oral candidiasis. *Carbohydr. Polym.* **2015**, *132*, 173–179. [[CrossRef](#)] [[PubMed](#)]
53. Tonglairoum, P.; Chuchote, T.; Ngawhirunpat, T.; Rojanarata, T.; Opanasopit, P. Encapsulation of plai oil/2-hydroxypropyl-beta-cyclodextrin inclusion complexes in polyvinylpyrrolidone (PVP) electrospun nanofibers for topical application. *Pharm. Dev. Technol.* **2014**, *19*, 430–437. [[CrossRef](#)] [[PubMed](#)]
54. Brewster, M.E.; Loftsson, T. The use of chemically modified cyclodextrins in the development of formulations for chemical delivery systems. *Pharmazie* **2002**, *57*, 94–101. [[PubMed](#)]
55. Celebioglu, A.; Uyar, T. Electrospinning of nanofibers from non-polymeric systems: Polymer-free nanofibers from cyclodextrin derivatives. *Nanoscale* **2012**, *4*, 621–631. [[CrossRef](#)]
56. Bilska, K.; Wojciechowska, N.; Alipour, S.; Kalembe, E.M. Ascorbic acid—the little-known antioxidant in woody plants. *Antioxidants* **2019**, *8*, 645. [[CrossRef](#)]
57. Trommer, H.; Neubert, R.H. Overcoming the stratum corneum: The modulation of skin penetration. A review. *Ski. Pharm. Physiol.* **2006**, *19*, 106–121. [[CrossRef](#)]
58. Barbero, A.M.; Frasc, H.F. Pig and guinea pig skin as surrogates for human in vitro penetration studies: A quantitative review. *Toxicol. Vitro.* **2009**, *23*, 1–13. [[CrossRef](#)]
59. Lee, K.E.; Ryu, J.J.; Jo, Y.K.; Yeo, H.; Kang, S. 2'-Fucosyllactose attenuates particulate matter-induced inflammation via inhibition of hypoxia-inducible factor in keratinocytes. *Biol. Pharm. Bull.* **2019**, *42*, 1620–1627. [[CrossRef](#)]
60. Dong, Y.M.; Liao, L.Y.; Li, L.; Yi, F.; Meng, H.; He, Y.F.; Guo, M.M. Skin inflammation induced by ambient particulate matter in China. *Sci. Total. Env.* **2019**, *682*, 364–373. [[CrossRef](#)]
61. Kim, J.H.; Kim, M.; Kim, J.M.; Lee, M.K.; Seo, S.J.; Park, K.Y. Afzelin suppresses proinflammatory responses in particulate matter-exposed human keratinocytes. *Int. J. Mol. Med.* **2019**, *43*, 2516–2522. [[CrossRef](#)]
62. Jin, S.P.; Li, Z.; Choi, E.K.; Lee, S.; Kim, Y.K.; Seo, E.Y.; Chung, J.H.; Cho, S. Urban particulate matter in air pollution penetrates into the barrier-disrupted skin and produces ROS-dependent cutaneous inflammatory response in vivo. *J. Derm. Sci.* **2018**, *91*, 175–183. [[CrossRef](#)] [[PubMed](#)]
63. Rajakariar, R.; Yaqoob, M.M.; Gilroy, D.W. COX-2 in inflammation and resolution. *Mol. Interv.* **2006**, *6*, 199–207. [[CrossRef](#)] [[PubMed](#)]
64. Corbel, M.; Belleguic, C.; Boichot, E.; Lagente, V. Involvement of gelatinases (MMP-2 and MMP-9) in the development of airway inflammation and pulmonary fibrosis. *Cell Biol. Toxicol.* **2002**, *18*, 51–61. [[CrossRef](#)] [[PubMed](#)]
65. Hannocks, M.J.; Zhang, X.; Gerwien, H.; Chashchina, A.; Burmeister, M.; Korpos, E.; Song, J.; Sorokin, L. The gelatinases, MMP-2 and MMP-9, as fine tuners of neuroinflammatory processes. *Matrix Biol.* **2019**, *75–76*, 102–113. [[CrossRef](#)]

66. Vandooren, J.; Van Damme, J.; Opdenakker, G. On the structure and functions of gelatinase B/matrix metalloproteinase-9 in neuroinflammation. *Prog. Brain Res.* **2014**, *214*, 193–206. [[CrossRef](#)]
67. Fathi-Azarbayjani, A.; Qun, L.; Chan, Y.W.; Chan, S.Y. Novel vitamin and gold-loaded nanofiber facial mask for topical delivery. *AAPS Pharmscitech* **2010**, *11*, 1164–1170. [[CrossRef](#)]
68. Krutmann, J.; Bouloc, A.; Sore, G.; Bernard, B.A.; Passeron, T. The skin aging exposome. *J. Derm. Sci.* **2017**, *85*, 152–161. [[CrossRef](#)]



© 2020 by the authors. Licensee MDPI, Basel, Switzerland. This article is an open access article distributed under the terms and conditions of the Creative Commons Attribution (CC BY) license (<http://creativecommons.org/licenses/by/4.0/>).